Supershort avalanche electron beam in SF$_6$ and krypton

Cheng Zhang (章程),[1] Victor F. Tarasenko,[2,3,4] Jianwei Gu (顾建伟),[1] Evgeni Kh. Baksht,[2]
Dmitry V. Beloplotov,[2,4] Alexander G. Burachenko,[2,4] Ping Yan (严萍),[1]
Mikhail I. Lomaev,[2,4] and Tao Shao (邵涛)[1,*]

[1]*Institute of Electrical Engineering, Chinese Academy of Sciences, Beijing 100190, China*
[2]*Institute of High Current Electronics, Russian Academy of Sciences, Tomsk 634055, Russia*
[3]*National Research Tomsk Polytechnic University, Tomsk 634050, Russia*
[4]*National Research Tomsk State University, Tomsk 634050, Russia*

Runaway electrons play an important role in the avalanche formation in nanosecond- and subnano-second- pulse discharges. In this paper, characteristics of a supershort avalanche electron beam (SAEB) generated at the subnanosecond and nanosecond breakdown in sulfur hexafluoride (SF$_6$) in an inhomogeneous electric field were studied. One pulser operated at negative polarity with voltage pulse amplitude of ∼130 kV and rise time of 0.3 ns. The other pulser operated at negative polarity with voltage pulse amplitude of 70 kV and rise time of ∼1.6 ns. SAEB parameters in SF$_6$ are compared with those obtained in krypton (Kr), nitrogen (N$_2$), air, and mixtures of SF$_6$ with krypton or nitrogen. Experimental results showed that SAEB currents appeared during the rise-time of the voltage pulse for both pulsers. Moreover, amplitudes of the SAEB current in SF$_6$ and Kr approximately ranged from several to tens of milliamps at atmospheric pressure, which were smaller than those in N$_2$ and air (ranging from hundreds of milliamps to several amperes). Furthermore, the concentration of SF$_6$ additive could significantly reduce the SAEB current in N$_2$-SF$_6$ mixture, but it slightly affected the SAEB current in Kr-SF$_6$ mixture because of the atomic/molecular ionization cross section of the gas had a much greater impact on the SAEB current rather than the electronegativity.

I. INTRODUCTION

Recently, great progress in the study of runaway electrons (RAEs) in high-pressure discharges has been achieved [1–4]. The development of measurement devices and methods has helped scientists learn more about the RAEs [5–6]. In the last decade, much attention has been paid to the definition of RAE parameters, characteristics of RAEs at breakdown in atmospheric pressure air, and the generation mechanism of RAEs in air, nitrogen and helium [1–9]. However, very little comprehensive data about RAEs in heavy gases is available. For instance, for sulfur hexafluoride (SF$_6$), which is usually used as an insulating medium, RAEs at breakdown in SF$_6$ have only obtained and reported by two scientific groups.

In Babich *et al.*'s paper, the generation of RAEs behind an anode foil at breakdown in SF$_6$ was first measured by the darkening of an X-ray film for detecting the RAEs [10]. The quantity of RAEs was estimated ∼10^8 per pulse, which was approximately one order of magnitude lower than that

in air. The temporal behavior of the RAEs was measured by using a scintillator and a photomultiplier with a time resolution no better than 3.5 ns. It was reported that the energy of RAEs in SF$_6$ was higher than that in air. Additionally, it was reported that the monoenergetic RAE beam, with anomalous energy, could be generated in both SF$_6$ and air [10–12]. The term "anomalous energy" herein refers to such electron energy that is higher than eU_m, where e is the charge of the electron, U_m is the maximum voltage across the discharge gap when RAEs generate. In those papers, it was proposed that the e-beam current in SF$_6$ was lower than that in air due to the attachment of electrons to SF$_6$, a strong electronegative gas [10–11].

Nevertheless, Tarasenko *et al.* achieved some different experimental results on RAEs. It was found that there were two or three groups of electrons with different energies in the RAE beam obtained downstream from the anode foil [13–15]. Moreover, under an optimal condition, the quantity of electrons with the anomalous energy was not more than 10% of the total number of the RAEs. They named the RAE beam behind the anode foil a "supershort avalanche electron beam" (SAEB) [16]. Baksht *et al.* first measured the SAEB by using a collector with time resolution of subnanosecond in nanosecond-pulse discharges sustained by the RADAN-220 pulser [8]. The SAEB was obtained in six different gases, including gases with a high atomic mass

(Kr, Xe). Their experimental results showed that the full width at half maximum (FWHMs) of SAEBs for SF_6 and other gases was about 100 ps at atmospheric pressure. Furthermore, this group compared the electron energy of the SAEB in air and SF_6. It was shown that, all other things (including amplitude and rise-time of voltage pulses, interelectrode distance, cathode configuration) being equal, the electron energy of the SAEB in air was higher than that in SF_6 [15].

According to the research performed by Mesyats *et al.*, all the energies of RAEs were not higher than eU_m at atmospheric pressure in air [5,17]. In these papers, it was pointed that RAEs with anomalous energy were not obtained in atmospheric pressure air when voltage pulses with a rise-time of subnanosecond were applied across the discharge gap, indicating no RAEs with anomalous energy in atmospheric air existed. Mesyats *et al.* failed to measure the SAEB in SF_6 in atmospheric-pressure discharges sustained by the RADAN-303 pulser [18]. This was mainly because the rise-time (~1.5 ns) of voltage pulses for the RADAN-303 pulser was slower than that (~0.5 ns) for the RADAN-220 pulser. However, because the intensity of SAEB in air was stronger than that in SF_6, the SAEB in air in the discharges sustained by the RADAN-303 pulser was measured.

Detailed investigation of the SAEB in SF_6 with higher time resolution (up to 90 ps) has been conducted [19–20]. It was found that the SAEB in SF_6 could be obtained at a pressure up to 2 atm, as well as its FWHM depended upon the pressure of SF_6 and the voltage pulse amplitude [15,19].

From all the statements about the RAEs at breakdown in SF_6 and air mentioned above, it can be concluded that there is no consensus regarding the characteristics of RAEs in air and heavy gases and their generation mechanism [1–28]. Therefore, it is necessary to carry out new experimental investigations for further research and compare the experimental results in order to eliminate misunderstandings. Note that the research on discharges in SF_6 has not only scientific importance, but also great practical importance, because SF_6 is widely used as insulating gas in high-voltage devices and a component of chemical gas lasers [29–31].

The objective of this work is to better understand the characteristics of SAEB, and to experimentally investigate and compare the characteristics of SAEB in heavy gases (including SF_6, krypton (Kr)) and their mixtures with nitrogen (N_2) and air at atmospheric pressure.

II. EXPERIMENTAL SETUP AND MEASUREMENT

Figure 1 shows the schematic of the experimental setup 1. The experiments were carried out on the setup, which consists of a SLEP-150M pulser, a transmission line, a gas diode and a measurement system [27–28]. The SLEP-150M pulser could provide voltage pulses with amplitude up to ~130 kV. The FWHM of the voltage pulses was
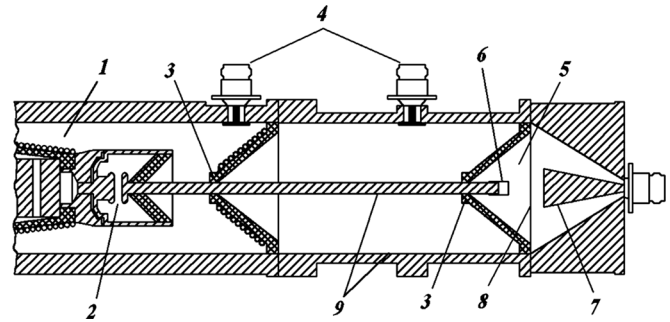
FIG. 1. Schematic picture of the SLEP-150M pulser with a gas-filled diode and a collector: (1) output section of pulser, (2) peaking spark gap, (3) insulators, (4) capacitive dividers, (5) gas filled diode, (6) cathode, (7) receiving part of the collector, (8) foil reinforced with a grid, (9) transmission line.

approximately 1 ns. The rise time of the voltage pulses depended on the peaking spark gap, and was 0.3 ns in the experiments. Note that the rise time was shorter than that for RADAN-220. Four capacitive dividers were installed into the transmission line. One of them was located near the gas diode and was used to measure the output voltage. The discharge current was measured by a shunt composed of chip resistors. These resistors with resistance of 0.038 Ohm were connected in series with the foil and were uniformly located at its circumference. There was a 1-cm-diameter hole in the center of the shunt. Metal grid with a transmittance of 14% was installed on the front side of the hole. The metal grid served as the anode. The cathode was a tube, which had a diameter of 6 mm and an edge thickness of 200 μm. The cathode edge was rounded. In the experiments, the interelectrode distance was 4 or 8 mm. Behind the metal grid, there was a 10-μm-thick aluminum foil, followed by a collector. The receiving part of the collector had a diameter of 20 mm. The time resolution of this collector was ~100 ps. It should be pointed out that only part of SAEB generated in the gas diode could be measured by the collector due to the hole in the center of the shunt separating some parts of the SAEB, and the metal grid and the aluminum foil attenuated some parts of the SAEB as well. Signals from the divider, the shunt and the collector were recorded using a digital oscilloscope DSO-X6004A (6 GHz, 20 GS/s).The discharge chamber was pumped with a forevacuum pump. The discharge chamber was filled with SF_6, Kr, N_2, air and mixtures of these gases. The pressures of these gases ranged from 0.001 atm to 3 atm.

The experimental setup 2 had a similar structure and arrangement as the experimental setup 1. Negative voltage pulses were generated by a VPG-30-200 pulser [19–20]. The output of the voltage pulses ranged from 30 to 200 kV, and it has a FWHM of 3–5 ns and a rise time of ~1.6 ns. All the experiments were carried out under a single-shot mode. The discharge was created in a tube-plane electrode. The tube electrode was connected to the output of the pulser and served as the cathode. It was made of a stainless steel foil

whose inner diameter was 6 mm and edge thickness was $\sim 100~\mu$m. The plane electrode was grounded and served as the anode. It was made of an aluminum foil whose thickness was 10 μm. The electrode distance ranged from 4 to 20 mm. The voltage applied at the electrodes was measured by using a capacitive divider, located at the end of the transmission line, with a division ratio was 1290:1. A collector was located behind the foil. The receiving part of the collector had a diameter of 40 mm. The time resolution of the collector was $\sim$0.5 ns. A Lecroy WR204Xi oscilloscope with a bandwidth of 2 GHz and a sampling frequency of 10 GS/s was used to record these signals.

III. EXPERIMENTAL RESULTS

A. Experimental results for setup 1

Figure 2 shows the typical waveforms of the voltage pulse from capacitive divider located near the gas diode, discharge current and SAEB current in SF₆ at atmospheric pressure. The experimental conditions were as follows: the incident wave's voltage was $\sim$130 kV, the interelectrode distance was 8 mm, and the gas diode was filled with SF₆. It could be observed that SAEB currents appeared during the rise-time of the voltage pulse and maximum of the SAEB current was obtained when the voltage across the gap began to decline. Meanwhile, the increase of the discharge current slowed. It should be pointed out that the oscillation of the voltage across the gap after the generation of the SAEB current was determined by the breakdown in the gap.

Figure 3 shows the dependence of the amplitude of the voltage across the gap and the SAEB current on the concentration of SF₆ in N₂-SF₆ mixture at atmospheric pressure as well as the dependence of the amplitude of the voltage across the gap and the SAEB current on the SF₆ pressure. The interelectrode distance was 4 mm. The amplitude of the SAEB current here was obtained after taking into account the transmittance of the metal grid.

When the concentration of SF₆ in N₂-SF₆ mixture increased from 1% to 10%, the SAEB current significantly decreased from 1.54 A to 0.25 A. However, after that, further increasing the concentration of SF₆ could no longer lead to a fast decrease of the SAEB current, and its amplitude was consistently near zero. However, increasing the concentration of SF₆ had little effect on the voltage across the gap. Thus, the SAEB could more likely be obtained in N₂-SF₆ mixture when the concentration of SF₆ was less than 10%.

In pure SF₆, the SAEB current increased when the SF₆ pressure decreased, which is consistent with the experimental results of our previous work [15,19]. Meanwhile, when the SF₆ pressure decreased, the voltage across the gap initially decreased until the pressure of SF₆ reached 0.1 atm, at which point the voltage across the gap began to increase while the SF₆ pressure was still decreasing. This leads to a minimum voltage across the gap obtained when the SF₆ pressure was 0.1 atm.

Figure 4 shows the dependence of the amplitude of the voltage across the gap and the SAEB current on the concentration of SF₆ in Kr-SF₆ and N₂-SF₆ mixtures at atmospheric pressure. Note that the difference in voltage

FIG. 2. Typical waveforms of the voltage pulse from capacitive dividers located near the gas diode (1), current through gap (2) and SAEB current (3) in SF₆ at atmospheric pressure. Interelectrode distance $d = 8$ mm.
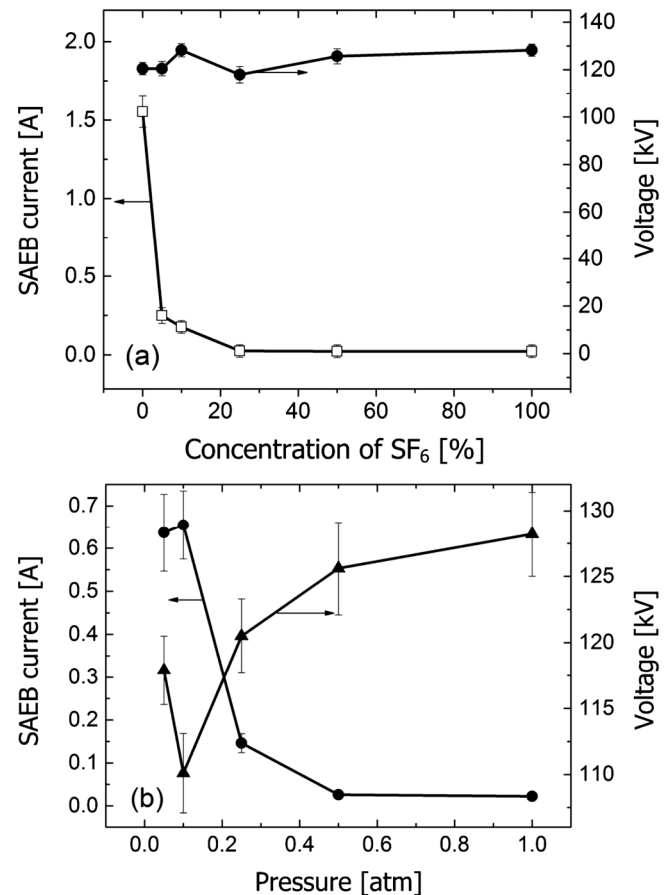
FIG. 3. Dependence of amplitude of voltage across the gap and SAEB current on the concentration of SF₆ in N₂-SF₆ mixture (a) and on the SF₆ pressure (b). Interelectrode distance $d = 4$ mm.

amplitude for each point in Figs. 3 and 4 was not larger than 10%, and the difference in amplitude of SAEB current was not higher than 20%. Furthermore, all other things being equal, the interelectrode distance was then increased to 8 mm. Similar to the experimental results for the inter-electrode distance of 4 mm were obtained, including the amplitude of the SAEB current decreasing when the SF_6 pressure increased, as well as the voltage across the gap slightly fluctuated with the increase of SF_6 pressure.
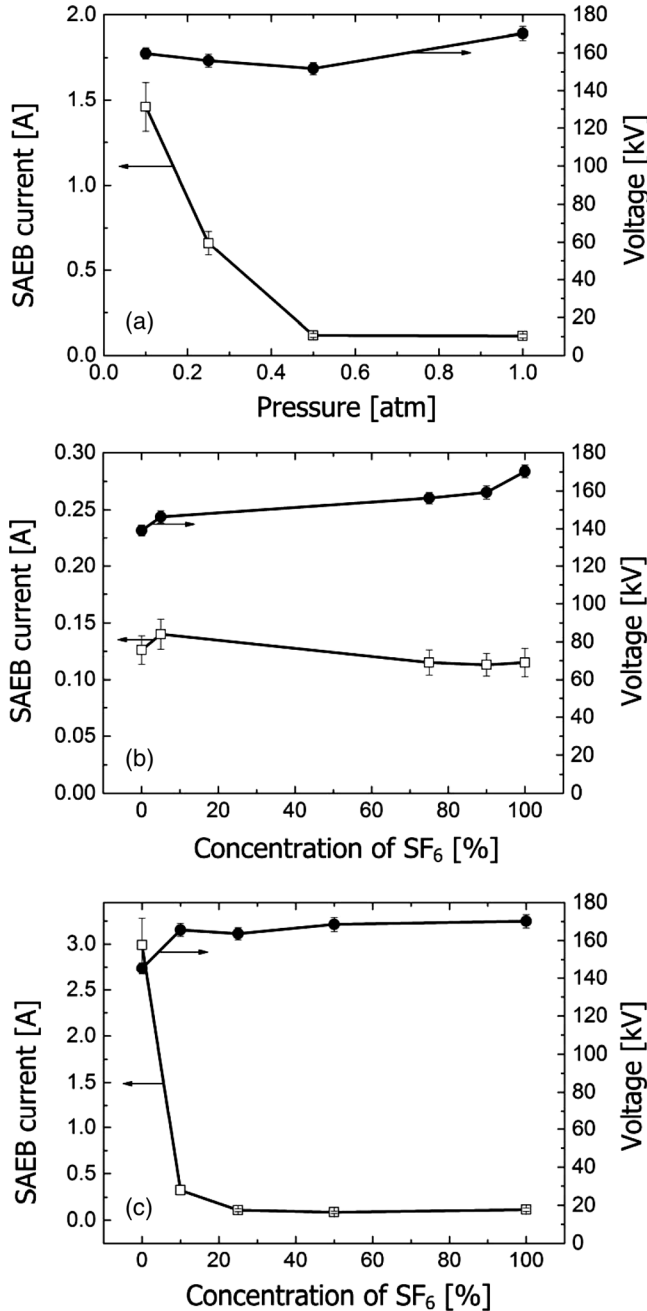
FIG. 4. Dependence of the voltage across the gap and SAEB current on SF_6 pressure (a) and SF_6 concentration in Kr-SF_6 (b) and N_2-SF_6 (c) mixtures at atmospheric pressure. Interelectrode distance $d = 8$ mm.

It was shown that the amplitude of the SAEB current significantly decreased when the concentration of SF_6 in N_2-SF_6 mixture increased from 0% to 10% at atmospheric pressure. When the concentration of SF_6 in N_2-SF_6 mixture exceeded 25%, the SAEB current declined to almost zero. However, the change of SF_6 concentration in N_2-SF_6 mixture had a very small influence on the maximum voltage across the gap.

Differently from the effect of SF_6 concentration in N_2-SF_6 mixture on the characteristics of the SAEB, both the amplitude of the SAEB current and the voltage across the gap were slightly influenced by the change of SF_6 concentration in Kr-SF_6 mixture. In our opinion, it was mainly because the electron energy lost in the excitation and ionization in SF_6 was much higher than that in N_2. Not like the explanation from Babich *et al.* [10–11], the effect of the strong electronegativity of SF_6 was very limited here. Thus, as the concentration of SF_6 in N_2-SF_6 mixture increased, more and more electron energy was consumed, leading to the decrease of the SAEB current. However, the electron energy lost in the excitation and ionization in SF_6 and Kr were almost the same, so the amplitude of SAEB current was slightly affected by the concentration of the SF_6 additive in Kr.

B. Experimental results for setup 2

Figure 5 shows the waveforms of the voltage across the gap and SAEB current in SF_6 at atmospheric pressure. The experimental conditions were as follows: the incident wave's voltage was about 70 kV, the gap was 12 mm, and the SF_6 pressures ranged from 0.003 atm to 1 atm. It could be seen that because the rise time of the setup 2 was longer than that of the setup 1, the breakdown voltage in Fig. 5 was lower than that in Fig. 2. The corresponding SAEB current for setup 2 was also smaller than that for setup 1. It was due to the short rise time and small interelectrode distance for setup 1. Note that the SAEB current appeared during the
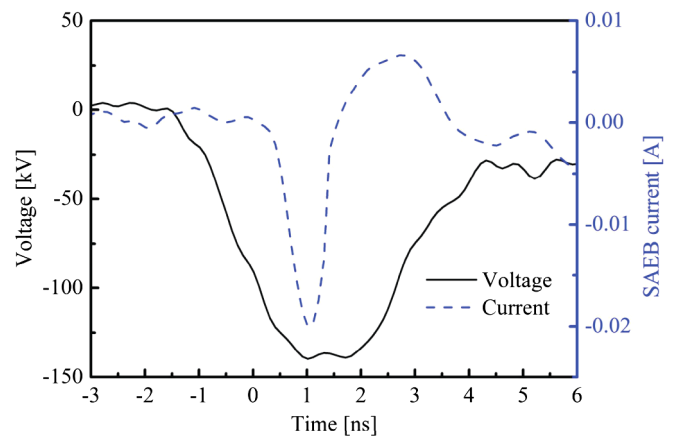
FIG. 5. Typical waveforms of the voltage pulse and SAEB current in SF_6 at atmospheric pressure. Interelectrode distance $d = 12$ mm.

rise-time of the voltage pulse and the maximum of the SAEB current was obtained when the voltage across the gap reached its maximum value.

Figure 6 shows the voltage across the gap and the SAEB current at different pressures in SF$_6$ and air. Although the rise time for setup 2 was longer than that for setup 1, it could be seen that the dependences of the voltage across the gap and SAEB current on the pressure in SF$_6$ for setup 2 were similar to those for setup 1. Furthermore, comparing the characteristics of RAEs between SF$_6$ and air, it could be found that at the same pressure, the voltage across the gap in air was lower than that in SF$_6$ and the corresponding amplitude of the SAEB current was higher than that in SF$_6$. Note that the amplitude of the SAEB current in air was about 13 times higher than that in SF$_6$ when the pressure was 0.01 atm, whereas the amplitude of the SAEB current in air was approximately 25 times higher than that in SF$_6$ when the pressure increased to 1 atm. This was mainly

FIG. 6. Dependence of amplitude of voltage across the gap (a) and SAEB current (b) on the pressure in SF$_6$ and air. Interelectrode distance $d = 12$ mm.

because the electron energy in excitation and ionization in SF$_6$ was much higher than that in air and nitrogen [29–31].

IV. DISCUSSION

Generally, the generation RAEs consists of four main stages: (i) the appearance of initial electrons, (ii) the mode transition into runaway electrons for part electrons, (iii) the generation of general RAEs, (iv) the ionization wave front arrival at the anode [1,7,13,15,19]. In the first stage, when the nanosecond high-voltage pulses are applied on the cathode, the electric field strength achieves sufficient value ($>10^7$ V/m) at the macro- and micro-inhomogeneities of the cathode, resulting in the appearance of initial electrons near the cathode and the development of electron avalanches. During this stage, the strong electronegativity of SF$_6$ has a slight effect on the generation of SAEB because of the high electric field strength. In the second stage, the heads of electron avalanches overlap with each other, and the electron avalanches do not reach critical size for forming streamers. At this moment, part of the initial electrons gain sufficient energy required for transiting into runaway mode. To determine the effect of electronegativity of gases at this stage, it is necessary to carry out theoretical modeling in future work. In the third stage, the number of runaway electrons increases due to electrons acceleration between the dense polarized plasma front (ionization wave front) and anode. These runaway electrons continuously move toward the anode. Such movement in the ionization wave front and in the gap would be affected by the negative charge of the avalanche heads and the anode applied voltage. The energy loss of electrons during collisions with gas molecules in SF$_6$ and Kr is significantly higher than in air and N$_2$, leading to amplitudes of SAEB current in air and N$_2$ being larger than those in SF$_6$ and Kr. Moreover, the voltage across the gap in air and N$_2$ is smaller than that in SF$_6$ and Kr. Note that the quantity of RAEs and the amplitudes of the SAEB current in SF$_6$ and Kr or in N$_2$ and air are approximately the same. In this case, the atomic/molecular ionization cross section of a gas plays an important role on the SAEB current. Although SF$_6$ and air have strong electronegativity and Kr and N$_2$ have no electronegativity, amplitudes of SAEB currents in SF$_6$ and Kr are not substantially different for the same conditions [19,32]. Thus, it can be seen that the electronegativity has less effect on the SAEB current than the atomic/molecular ionization cross section. In the final stage, the ionization wave front reaches anode. The electric field strength distribution becomes more uniform and SAEB generation finishes, as well voltage across the gap decreases.

V. CONCLUSION

In this paper, characteristics of the SAEB current in heavy gases (SF$_6$ and Kr) were investigated. The
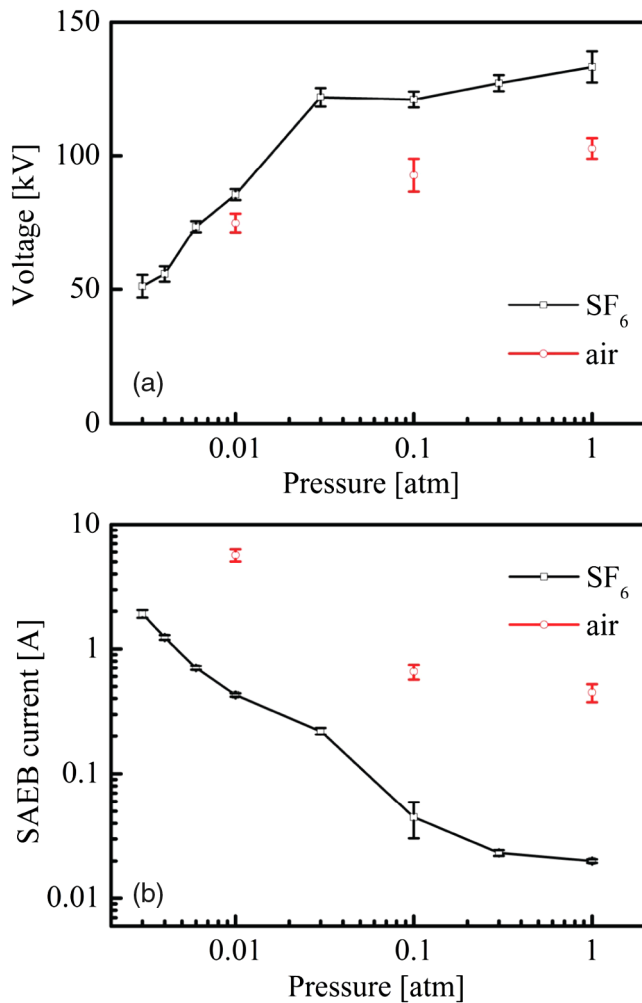
experimental results showed that SAEB currents were obtained in SF_6, Kr, N_2, air, and mixtures of these gases at atmospheric pressure in discharges sustained by voltage pulses with both subnanosecond and nanosecond rise times. The SAEB currents appeared during the rise-time of the voltage pulse. The amplitudes of the SAEB current in SF_6 and Kr were significantly lower than those in N_2 and air. Furthermore, SF_6 concentration in N_2-SF_6 mixture prominently affected the amplitude of SAEB current and the voltage across the gap, but the SF_6 concentration in Kr-SF_6 mixture only slightly affected the amplitude of SAEB current. The effect of the SF_6 concentration in different gas mixture on the SAEB current was not only due to the strong electronegativity of SF_6. In fact, such influence by electronegativity was very limited. It could be shown from our experimental results that the atomic/molecular ionization cross section of a gas may have a much greater impact on the SAEB current. In the case of N_2-SF_6 mixture, the electron energy lost in the excitation and ionization in SF_6 was much higher than that in N_2, however, in the case of Kr-SF_6 mixture, the electron energy lost in the excitation and ionization in SF_6 and Kr were almost the same. Therefore, the amplitude of SAEB current was slightly affected by the concentration of the SF_6 additive in Kr-SF_6 mixture. As to the energy of RAEs in SF_6 and Kr, a detailed investigation of the energy of RAEs can be caclulated by reconstructing from attenuation at the anode foils using different thicknesses. Detailed results will be given in the nearest future.

ACKNOWLEDGMENTS

[1] V. F. Tarasenko, E. Kh Baksht, A. G. Burachenko, I. D. Kostyrya, M. I. Lomaev, and D. V. Rybka, IEEE Trans. Plasma Sci. **37**, 832 (2009).

[2] A. V. Gurevich, G. A. Mesyats, K. P. Zybin, M. I. Yalandin, A. G. Reutova, V. G. Shpak, and S. A. Shunailov, Phys. Rev. Lett. **109**, 085002 (2012).

[3] V. Dudnikov and R. P. Johnson, Phys. Rev. Accel. Beams **14**, 054801 (2011).

[4] T. Shao, V. F. Tarasenko, C. Zhang, E. K. Baksht, D. Zhang, M. V. Erofeev, C. Ren, Y. V. Shutko, and P. Yan, J. Appl. Phys. **113**, 093301 (2013).

[5] G. A. Mesyats, M. I. Yalandin, A. G. Reutova, K. A. Sharypov, V. G. Shpak, and S. A. Shunailov, Plasma Phys. Rep. **38**, 29 (2012).

[6] D. Levko, Y. E. Krasik, V. F. Tarasenko, D. V. Rybka, and A. G. Burachenko, J. Appl. Phys. **113**, 196101 (2013).

[7] T. Shao, V. F. Tarasenko, C. Zhang, A. G. Burachenko, D. V. Rybka, I. D. Kostyrya, M. I. Lomaev, E. Kh. Baksht, and P. Yan, Rev. Sci. Instrum. **84**, 053506 2013.

[8] E. Kh. Baksht, M. I. Lomaev, D. V. Rybka, and V. F. Tarasenko, Tech. Phys. Lett. **32**, 948 (2006).

[9] C. Zhang, V. F. Tarasenko, T. Shao, E. Kh. Baksht, A. G. Burachenko, P. Yan, and I. D. Kostyrya, Laser Part. Beams **31**, 353 (2013).

[10] L. P. Babich and T. V. Loiko, *Tech. Phys.* **61**, 153 (1991).

[11] L. P. Babich and T. V. Loiko, Dokl. Phys. **50**, 241 (2005).

[12] L. P. Babich and T. V. Loiko, *Tech. Phys.* **55**, 956 (1985).

[13] E. Kh. Baksht, A. G. Burachenko, V. Y. Kozhevnikov, A. V. Kozyrev, I. D. Kostyrya, and V. F. Tarasenko, J. Phys. D **43**, 305201 (2010).

[14] A. V. Kozyrev, V. Yu. Kozhevnikov, M. S. Vorobyev, E. Kh. Baksht, A. G. Burachenko, N. N. Koval, and V. F. Tarasenko, Laser Part. Beams **33**, 183 (2015).

[15] E. Kh. Baksht, A. G. Burachenko, M. V. Erofeev, M. I. Lomaev, D. V. Rybka, D. A. Sorokin, and V. F. Tarasenko, Laser Phys. **18**, 732 (2008).

[16] V. F. Tarasenko, V. M. Orlovskii, and S. A. Shunailov, Russ. Phys. J. **46**, 325 (2003).

[17] G. A. Mesyats, A. G. Reutova, K. A. Sharypov, V. G. Shpak, S. A. Shunailov, and M. I. Yalandin, Laser Part. Beams **29**, 425 (2011).

[18] G. A. Mesyats, S. D. Korovin, K. A. Sharypov, V. G. Shpak, S. A. Shunailov, and M. I. Yalandin, Tech. Phys. Lett. **32**, 18 (2006).

[19] C. Zhang, V. F. Tarasenko, T. Shao, D. V. Beloplotov, M. I. Lomaev, D. A. Sorokin, and P. Yan, Laser Part. Beams **32**, 331 (2014).

[20] C. Zhang, H. Ma, T. Shao, Q. Xie, W. Yang, and P. Yan, Acta Phys. Sin. **63**, 085208 (2014).

[21] D. Levko, V. T. Gurovich, and Y. E. Krasik, J. Appl. Phys. **111**, 013306 (2012).

[22] T. Shao, V. F. Tarasenko, C. Zhang, M. I. Lomaev, D. A. Sorokin, P. Yan, A. V. Kozyrev, and E. Kh. Baksht, J. Appl. Phys. **111**, 023304 (2012).

[23] D. Levko, V. T. Gurovich, and Y. E. Krasik, J. Appl. Phys. **111**, 123303 (2012).

[24] S. N. Ivanov, J. Phys. D **46**, 285201 (2013).

[25] M. I. Lomaev, D. V. Beloplotov, V. F. Tarasenko, and D. A. Sorokin, IEEE Trans. Dielectr. Electr. Insul. **22**, 1833 (2015).

[26] B. D. Huang, K. Takashima, X. M. Zhu, and Y. K. Pu, J. Phys. D **47**, 422003 (2014).

[27] T. Shao, V. F. Tarasenko, W. Yang, D. V. Beloplotov, C. Zhang, M. I. Lomaev, P. Yan, and D. A. Sorokin, Plasma Sources Sci. Technol. **23**, 054018 (2014).

[28] V. F. Tarasenko, I. D. Kostyrya, E. K. Baksht, and D. V. Rybka, IEEE Trans. Dielectr. Electr. Insul. **18**, 1250 (2011).

[29] M. Bortnik, *The Physical Properties and the Electrical Strength of Sulfur Hexafluoride* (Energoatomizdat, Moscow, 1998).

[30] R. W. F. Gross and J. F. Bott, *Handbook of Chemical Lasers* (Wiley-Interscience, New York, 1976).

[31] A. N. Panchenko, M. I. Lomaev, N. A. Panchenko, V. F. Tarasenko, and A. I. Suslov, Proc. SPIE Int. Soc. Opt. Eng. **9255**, 92552V (2015).

[32] D. Levko and Y. E. Krasik, J. Appl. Phys. **112**, 113302 (2012).